Monthly Notices
of the
ROYAL ASTRONOMICAL SOCIETY

MNRAS **461,** 3620–3629 (2016)
Advance Access publication 2016 June 30

doi:10.1093/mnras/stw1570

New insights on the formation of nuclear star clusters

Nicolas Guillard,[1,2]★ Eric Emsellem[2,3] and Florent Renaud[4]

[1]*Excellence Cluster Universe, Boltzmannstr. 2, D-85748 Garching, Germany*
[2]*European Southern Observatory, Karl-Schwarzschild-str. 2, D-85748 Garching, Germany*
[3]*Université de Lyon 1, CRAL, Observatoire de Lyon, 9 av. Charles André, CNRS, UMR 5574; ENS de Lyon, F-69230 Saint-Genis Laval, France*
[4]*Department of Physics, University of Surrey, Guildford GU2 7XH, UK*

Accepted 2016 June 27. Received 2016 June 17; in original form 2016 May 24

ABSTRACT

Nuclear clusters (NCs) are common stellar systems in the centres of galaxies. Yet, the physical mechanisms involved in their formation are still debated. Using a parsec-resolution hydrodynamical simulation of a dwarf galaxy, we propose an updated formation scenario for NCs. In this 'wet migration scenario', a massive star cluster forms in the gas-rich disc, keeping a gas reservoir, and growing further while it migrates to the centre via a combination of interactions with other substructures and dynamical friction. A wet merger with another dense cluster and its own gas reservoir can occur, although this is not a prerequisite for the actual formation of the NC. The merging process does significantly alter the properties of the NC (mass, morphology, star formation history), also quenching the ongoing local star formation activity, thus leading to interesting observational diagnostics for the physical origin of NCs. A population of lower mass clusters co-exist during the simulation, but these are either destroyed via tidal forces, or have high angular momentum preventing them to interact with the NC and contribute to its growth. The proposed updated scenario emphasizes the role of gas reservoirs associated with the densest star clusters formed in a gas-rich low-mass galaxy.

Key words: methods: numerical – Galaxy: evolution – Galaxy: nucleus.

1 INTRODUCTION

Nuclear star clusters (NCs) are present in a wide variety of galaxies, from early (e.g. Carollo, Stiavelli & Mack 1998; Turner et al. 2012; den Brok et al. 2014) to late-type galaxies (e.g. Böker et al. 2002; Georgiev & Böker 2014; Carson et al. 2015). Observational studies with the *Hubble Space Telescope* show that about 75 per cent of spiral and dwarf elliptical galaxies have a prominent NC (Côté et al. 2006; Seth et al. 2006, 2008; Neumayer & Walcher 2012). NCs have typical sizes of a few to a few tens of parsecs and a mass from 10^4 to 10^8 $M_\odot$ (e.g. Georgiev & Böker 2014), which rank them among the densest stellar objects in the Universe. The mass of NCs roughly scales with the galactic host properties such as the galactic mass, the velocity dispersion of the spheroidal component or and the total galactic luminosity (e.g. Ferrarese et al. 2006; Rossa et al. 2006; Graham 2012; Scott & Graham 2013; Georgiev et al. 2016). Understanding the physical origins of the properties of NC could thus shed new lights on the galaxy evolution.

To date, two main formation scenarios have been proposed (see top and middle rows of Fig. 1).

(i) *In situ* (Milosavljević 2004): gas falls on to the galactic centre which subsequently triggers star formation in the central few parsecs and forms the NC.

(ii) Migration (Tremaine, Ostriker & Spitzer 1975): a massive cluster forms, then migrates towards the centre by dynamical friction. This process is potentially followed by dry mergers (i.e. gas free) with other clusters (Andersen et al. 2008; Antonini 2013).

These formation scenarios imprint specific signatures on the properties of NCs. Probing the galaxy properties or examining the above-mentioned scaling relations should thus help us to disentangle between the various formation scenarios. The power-law relation between the mass of the NC and the velocity dispersion of the galaxy host observed by Ferrarese et al. (2006) is not reproduced by the *in situ* scenario (see analytical model Antonini 2013), while predictions from the migration model, including a dry-merger step, seem to be more successful (Antonini 2013; Arca-Sedda & Capuzzo-Dolcetta 2014). Dynamical simulations from Hartmann et al. (2011) also show that the mergers of star clusters in models tuned for NGC 4244 and M33 retrieve the properties expected from the scaling relations.

More recent studies emphasize the fact that these two scenarios are not exclusive and likely contribute together to build the properties of the NC (e.g. den Brok et al. 2014; Cole et al. 2016). Hartmann et al. (2011) points out that despite the fact that properties induced

★ E-mail: nguillar@eso.org

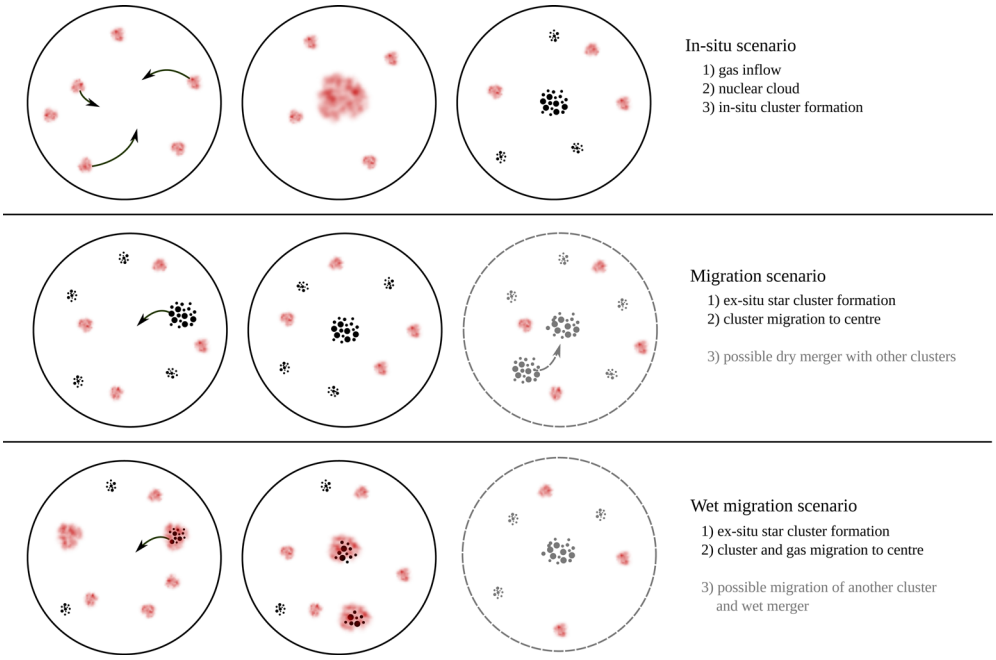

Figure 1. Schematics representation of NC scenarios from the literature and the one proposed in this work.

by cluster mergers are in agreement with observations, *in situ* star formation would still contribute for ∼50 per cent of the mass of the NC. Semi-analytic models by Antonini, Barausse & Silk (2015) lead to similar conclusions showing that stars formed *in situ* contribute to a large fraction (up to 80 per cent) of the total NC mass.

To further investigate the diverse origins of stellar population in NCs, we present a self-consistent hydrodynamical model of NCs formation in its galactic context. Using a parsec-resolution hydrodynamical simulations of a gas-rich dwarf galaxy, we propose a new scenario for the formation of NC (see bottom panel of Fig. 1) based on *ex situ* formation of massive clusters, their continuous growth, migration to the galactic centre, potentially followed by a *wet* merger with other clusters bringing their own gas reservoirs.

In Section 2, we describe the numerical methods. The formation scenario of the NC is described in Section 3. We show the interaction between the NC and the galactic cluster population in Section 4 and finally discuss the implications of this new scenario in Section 5.

2 NUMERICAL TOOLS AND CONVERGENCE

We run hydrodynamical simulations of an isolated dwarf galaxy using the Adaptive Mesh Refinement (AMR) code RAMSES (Teyssier 2002). We define three types of particles: the dark matter (DM), the stars included in the initial conditions (hereafter referred to as primitive stars), and stars we formed during the course of the simulations (hereafter referred to as new stars). The code solves the equations of motion with a particle-mesh scheme. The code uses a softening of the gravitational acceleration for the DM and primitive stars of 7 pc, while the softening for the new stars is the local resolution of the AMR grid, which is specific to each simulation (see Table 1 in Section 2.1). For the gas, the code solves the Euler equations on the AMR grid, allowing the densest regions to be refined while keeping a low resolution on more diffuse media. To avoid the artificial fragmentation of the densest regions, we add a pressure floor that ensures that a thermal Jeans length is always resolved by at least four cells. The physical ingredients we use in this simulation are similar to the ones used in Renaud, Bournaud & Duc (2015).

Table 1. Initial conditions.

Box length (kpc)		30	
AMR coarse level		8	
AMR finest level	11	12	13
Highest resolution (pc)	14.6	7.3	3.7
DM Halo			
Virial mass ($\times 10^9$ $M_\odot$)		100	
Virial radius (kpc)		120	
Cut radius (kpc)		15	
Concentration		16	
Profile		Navarro–Frenk–White	
Number of particles ($\times 10^5$)		37.5	
Primitive stars			
Mass ($\times 10^9$ $M_\odot$)		1	
Profile		Exponential	
Scale radius (kpc)		1	
Cut radius (kpc)		7.5	
Scaleheight (pc)		250	
Cut height (pc)		750	
Number of particles ($\times 10^5$)		15	
Gas			
Mass ($\times 10^9$ $M_\odot$)		2.3	
Profile		Exponential	
Scale radius (kpc)		1.65	
Cut radius (kpc)		7.5	
Scaleheight (pc)		165	
Cut height (pc)		750	
Average number of cells ($\times 10^6$)		2.4	

The size of the simulated volume is of 30 × 30 × 30 kpc^3, with the least resolved cells spanning 120 pc. We run a set of three simulations in which we vary the maximal resolution from 15 pc^3 to 3.5 pc^3 (see Table 1). The galaxy is modelled in isolation, thus neglecting the cosmological context. The simulations have been run

on the C2PAP facilities (Excellence Cluster, Garching) for about 1 million CPU-hours on 512 cores.

The gas is heated by ultraviolet radiation and cooled down by atomic cooling tabulated at solar metallicity (Courty & Alimi 2004). The minimal temperature reached is of 200 K.

Star formation follows the Schmidt law: $\rho_{\rm SFR} = \epsilon\rho/t_{\rm ff} \propto \epsilon\rho^{3/2}$ where ρ is the gas density, ϵ is the dimensionless efficiency of the star formation and $t_{\rm ff} = \sqrt{3\pi/(32\,G\rho)}$ is the free-fall time. This only concerns densities higher than a given threshold. We set an efficiency of 2 per cent and a density threshold of 100 cm^{-3}, so that the star formation rate (SFR) of the dwarf is about 0.1 $M_\odot$. This corresponds to the rates observed for galaxies of $\sim 10^9$ $M_\odot$ at redshift $z = 2$–3 which is the type of galaxies we model in this work (e.g. Behroozi, Wechsler & Conroy 2013). The stellar particles have a mass of 130 $M_\odot$.

The stellar feedback recipes we used are described in Renaud et al. (2013). Photoionization is modelled by creating a Strömgren sphere around massive stars (20 per cent of the stars mass explode as SNe) younger than 10 Myr. The radius of the sphere depends on the ambient gas density and the time-varying stellar luminosity. The interstellar medium (ISM) in the sphere is heated up to 4×10^4 K. In the bubble, the code injects momentum-driven feedback in the form of radial velocity kicks to model radiative pressure. Type II supernova (SN) feedback is implemented as a Sedov blast wave (see Dubois & Teyssier 2008 for details). SN injects 10^{51} erg in a kinetic form. Feedback from a potential active galactic nucleus is not included in these simulations.

2.1 Initial conditions and final state

Galaxies with stellar mass of $\sim 10^9$–10^{10} $M_\odot$ have the highest fraction of nucleated galaxies (Pfeffer et al. 2014), and we therefore set the total baryonic mass of our galaxy model in this range, namely to 3.3 10^9 $M_\odot$. Taking conditions representative of redshift $z \sim 2$–3 low-luminosity galaxies, we set the gas mass fraction to 70 per cent of the baryonic mass (Daddi et al. 2010), the stellar and gaseous masses being 10^9 and 2.3×10^9 $M_\odot$, respectively. The DM halo has a mass of 10^{11} $M_\odot$, following the scaling relation between DM halo and stellar disc from Ferrero et al. (2012). We model the DM halo with a Navarro–Frenk–White profile (Navarro, Frenk & White 1996) that has a concentration of 16 and a virial radius of 120 kpc. We truncate the halo at a radius of 15 kpc since we focus on the central regions of the galaxy.

At $t = 0$, our simulation volume is composed of both gaseous and stellar exponential discs embedded in a DM halo. We use the code PYGME (Python Multiple Gaussian Expansion) to generate the stellar component, the DM and gas. This code makes use of the Multi-Gaussian Expansion method (Monnet, Bacon & Emsellem 1992; Emsellem, Monnet & Bacon 1994), and spatially decomposes the mass of the galaxy in a set of Gaussian functions. We used a total of 26 Gaussians to generate the galaxy components: eight for the DM Halo, nine for the stellar disc and nine for the gas disc. The velocities of the particles are derived via the Jeans equations considering all components (gas, stars, DM) for the gravitational potential. The gas particles are then replaced by AMR cells. The initial properties of the galaxy are summarized in Table 1, and Fig. 2 displays the initial rotation profiles of the galaxy and of its components.

Star formation and feedback are not active at the beginning of the simulations. We progressively increase the refinement level of the grid. After a relaxation phase of 80 Myr we activate the SF and the feedback. After another 15 Myr of evolution, the simulation

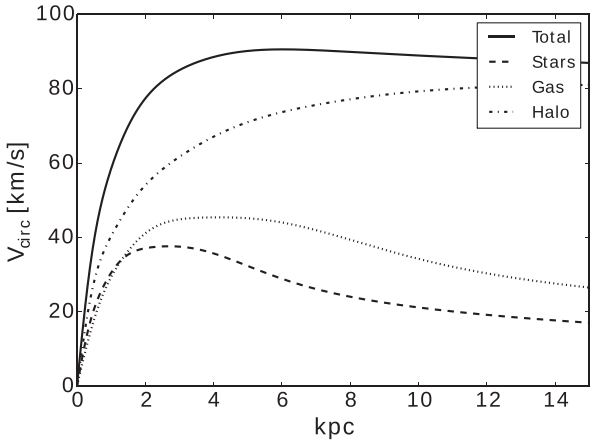

Figure 2. Rotation curves of the galactic components at $t = 0$ Myr.

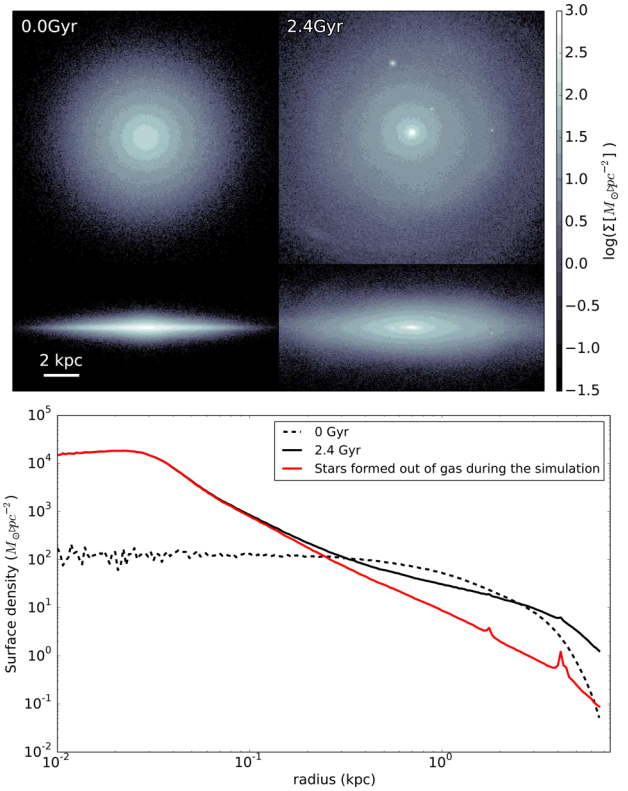

Figure 3. Top: face-on and edge-on surface density maps of all stars at the beginning (left) and at the end (right) of the simulation. Bottom: radial profile of the surface density of the galaxy at the beginning (dashed) and the end (solid) of the simulation. The new stars (red) dominate the central hundred parsecs.

reaches the maximum spatial resolution with all physical processes activated. We then let the system evolve for ∼2.4 Gyr.

At the end of the simulation, our galaxy has a stellar and gaseous mass of 1.5×10^9 and 3.1×10^8 $M_\odot$, respectively, and an NC has formed with a surface density of 2×10^4 $M_\odot$ pc^{-2}(see right-hand panel of Fig. 3).

We detect three smaller clusters orbiting around the nucleus with a period of a few hundreds Myr and orbital eccentricity between 0.3 and 0.6. The radial profile of the galactic surface density can be decomposed in three parts: the central region ($R < 200$ pc) which is dominated by new stars, a transition range for $0.2 < R$[kpc] < 1

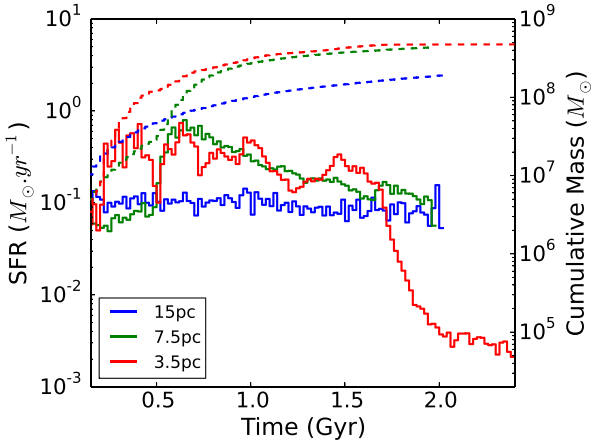

Figure 4. Cumulative mass of new stars (dashed) and SFR (filled) for simulations at resolutions of 15 pc (blue), 7.5 pc (green) and 3.5 pc (red). At t∼1.7 Gyr, a merger between two massive clusters occurs, coinciding with a sharp drop of the SFR.

and the outer part of the galaxy that exhibits an exponential profile with a scaling radius of 1.7 kpc.

2.2 Numerical convergence

When increasing the resolution, we have access to denser regimes of gas, which thus potentially increases the SFR. This increase is however regulated by feedback. We tested the efficiency in providing numerical convergence by running two additional otherwise identical simulations with maximum resolutions of 15 and 7.5 pc, respectively. Considering the complex evolution in the early stages of these gas-rich simulations, it is not relevant to compare the local details (star formation distribution, high-frequency features, etc) of each simulation. Still, it is important to figure out if the global properties do converge. Fig. 4 thus shows that the SFR is quantitatively different between the 15 and 7.5 pc resolution simulations. The former has an almost constant SFR, while the latter shows a rapid increase within the first 500 Mr and a steady decrease hereafter. In that context, the 3.5 pc resolution simulation shows a very similar behaviour, even though the higher resolution allows us to capture higher gas densities. This is confirmed by the fact that for the cumulative mass of new stars, convergence in the final stellar mass seems to occur between 7.5 and 3.5 pc. In short, the simulations at 7.5 and 3.5 pc form about the same amount of stellar mass (4.8×10^8 M$_\odot$) by the end of the simulation. In the rest of the paper, we thus focus on the simulation at the highest resolution, i.e. 3.5 pc.

2.3 Clusters detection

To detect star clusters, we use the friend-of-friend algorithm HOP (Eisenstein & Hut 1998). With this method, clusters are defined as overdensities regions above a given threshold. Namely, a cluster is detected when the peak of the local stellar density exceeds 1.5 M$_\odot$ pc^{-3}. Two clusters are then merged if the saddle density between them is higher than 1 M$_\odot$ pc^{-3}. The clusters properties can be significantly affected by the choice of parameters in this algorithm. Lowering the densities would obviously result into a contamination from the background stars, while increasing it would lead to more compact (detected) clusters. We test that changing the detection parameters by a factor of 2 slightly affects the derived properties of the clusters, but does not alter the conclusions of the paper.

3 FORMATION OF NC

Based on the simulation, we propose a new scenario for the formation of NCs. This 'wet migration' scenario consists of two main phases: the formation, growth and migration of a massive cluster towards the centre of the galaxy during which the cluster retains part of its gas, followed by a potential merger with another cluster.

3.1 Formation by migration

The cluster seed of our NC (named Cluster1) forms 1.1 kpc away from the galactic centre, at $t = 562$ Myr. At this stage, gas is still the major baryonic component of the galaxy disc, which has a rather irregular structure (see Fig. 5). A variety of clusters also form at the same epoch, with masses ranging from 10^5 to 10^7 M$_\odot$. Cluster1 collapses out of a clump of $\sim 2 \times 10^7$ M$_\odot$ (∼0.8 per cent of the galactic gas mass, see top panel of Fig. 6). The initial cluster has a stellar mass of 2×10^4 M$_\odot$, and converging flows supply the cluster with gas (see the gas velocity field in Fig. 6). The gravitational potential of Cluster1 is deep enough to retain this reservoir, keeping a relatively constant mass of gas ($2–3 \times 10^7$ M$_\odot$) in its vicinity despite its stellar feedback. Sustained star formation makes Cluster1 steadily grow in mass (see the solid lines in Fig. 7). Cluster1 also grows in size from ∼12 to 30–40 pc.

We can split the growth of Cluster1 into two phases.

(1) A rapid growth during the first 100 Myr. The gas dominates the mass budget within 200 pc.
(2) A slower growth in the following 800 Myr during which the mass of Cluster1 dominates the environment over the gas reservoir.

During the first phase, the amount of gas (>10^7 M$_\odot$) remains higher or of the same order of magnitude than the mass of Cluster1 (see Fig. 7). Variations of the gas reservoir mass have a strong impact on the mass growth rate of Cluster1: a decrease of the reservoir mass stops the growth (e.g. at $t' = 60$ Myr where t' is the relative time after the cluster formation) and its refilling accelerates it (e.g. at $t' = 100$ Myr). The refilling occurs both by local infall and during interactions with another dense cluster bringing its own gas. The decrease is mostly due to star formation and to SN blasts from the cluster itself or its neighbours. Fig. 8 shows that, since its formation, Cluster1 is one of the main contributors to the global SFR.

Fig. 9 shows that Cluster1 migrates towards the centre relatively slowly. Indeed, it takes 350 Myr to Cluster1 to cover a radial distance of 1.2 kpc at $t < 900$ Myr. Multiple interactions between Cluster1 and the surrounding structures slightly affect its orbits, and disturbs its migration towards the galactic centre.

SNe also have an impact on the orbital evolution of the cluster. For example, at $t = 730$ Myr ($t' = 170$ Myr in relative time), Cluster1 experiences a burst of star formation (see Fig 8). The newly formed stars slowly drift away from the remaining gas clump (due to asymmetric drift e.g. Renaud et al. 2013). 10 Myr later, SNe feedback inject energy into the ISM, forming a bubble which is therefore off-centred with respect to the gas clump (see Fig. 10). Since the gas represents a significant fraction of the local mass budget (52 per cent at that time for Cluster1, see Fig. 7), the local gravitational potential is significantly altered when the gas is expelled. As a result, Cluster1 gets a velocity kick which increases its orbital eccentricity, and sends it away from the galactic centre (see Fig. 9). About 50 Myr later, the cluster reaches its apocentre

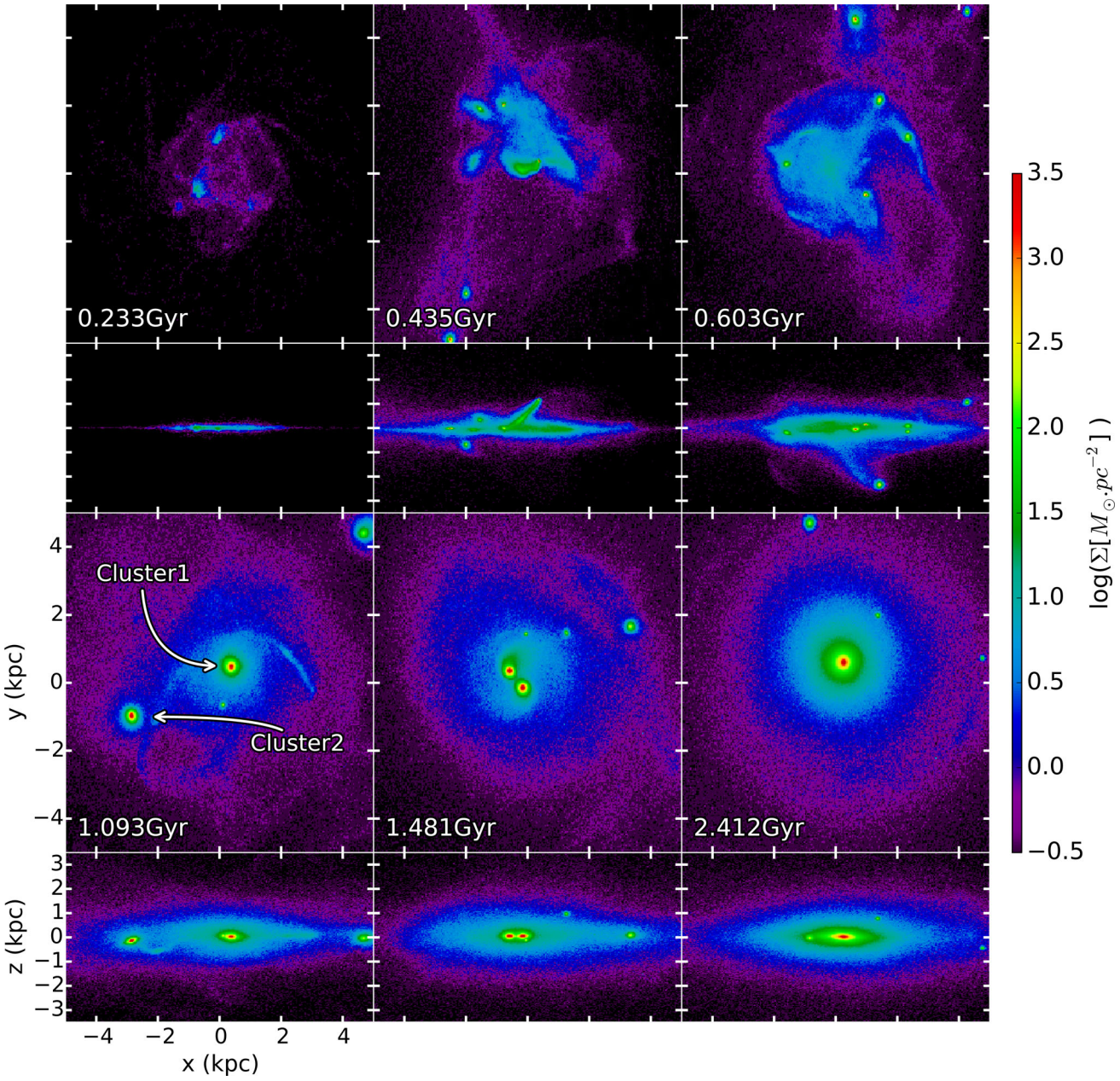

Figure 5. Surface density of stars that have been formed during the simulation. Cluster1 is the NC's seed. Cluster2 is the second most massive cluster in the simulation. It merges with Cluster1 at $t = 1.7$ Gyr.

and moves back towards the centre, reaching this time a smaller galactocentric distance ($d = 180$ pc at $t = 900$ Myr). At that stage, the cluster represents 67 per cent of the galactic central (r<500 pc) mass. It interacts with the stellar and gaseous material in the central region of the galaxy, which makes the galactic centre ill-defined. Nevertheless, the orbit of Cluster1 remains close to the centre of the global potential so that we can then consider Cluster1 as an NC.

3.2 NC–cluster merger

Another massive (4×10^7 M$_\odot$) cluster (Cluster2) evolves alongside Cluster1. It forms in a different environment (see bottom panel of Fig. 6) in the external region of the galaxy ($d = 3.8$ kpc, $t = 360$ Myr) where the stellar and gas densities are much lower. The ISM around Cluster2 is slightly less turbulent than around Cluster1 (Mach number of 0.33 and 0.66, respectively, on a scale of ∼240 pc). The early mass evolution of Cluster2 is similar to that of Cluster1 (see Fig. 7). Fig. 8 shows that Cluster2 is another important contributor to the overall SFR in the galaxy. We also note that the stellar mass dominates Cluster2 300 Myr after its formation, like Cluster1. Cluster1 and Cluster2 are thus initially in the same mass regime and share similar properties, while formed in rather different environments.

Fig. 9 shows that after interactions with the substructures in the galactic disc ($t < 950$ Myr), Cluster2 loses angular momentum and progressively migrates towards the centre. We estimate that the dynamical friction time is ∼1 Gyr (Chandrasekhar 1943; Mo, van den Bosch & White 2010), which is consistent with the time Cluster2 takes to reach the central region of the galaxy. At $t = 1.7$ Gyr, Cluster2 merges with the NC (initially Cluster1, which migrated earlier).

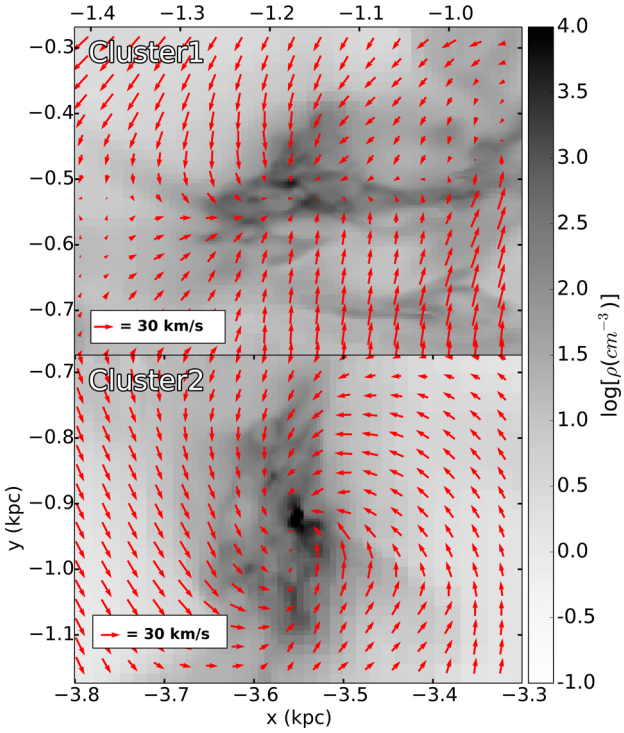

Figure 6. Maps of gas density at the earliest detection of the two most massive clusters in the galaxy. Cluster1 (top) forms the NC by migration, while Cluster2 (bottom) merges later with the NC. The velocity field in the (x,y) disc plane is shown with red arrows.

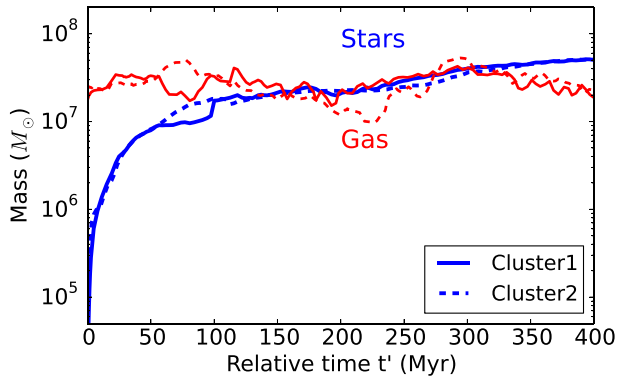

Figure 7. In blue: stellar mass of Cluster1 (solid) and of the second most massive cluster Cluster2 (dashed) starting at their respective first detection. In red: gas mass within 200 pc around the clusters. $t' = 0$ corresponds to the respective earliest detection epoch of the clusters. At $t' = 100$ Myr, Cluster1 merges with another cluster which rapidly increases its mass.

The resulting stellar system has a half-mass radius of ∼35 pc and a mass of 1.8×10^8 M$_\odot$ (see bottom-right row of Fig. 5). Because of the transfer of orbital momentum from Cluster2 to the stars of the merger, the resulting NC is flattened in the orbital plane of the interaction (which coincides with the plane of the galactic disc), with an axis ratio of 0.4.[1]

After the merger, the SFR drops by almost two orders of magnitude (see Fig. 8). Fig. 11 shows the evolution of the gas density

[1] We estimate the height and radius using isosurface density contours of 10^3 M$_\odot$ pc^{-2} in its edge-on projection.

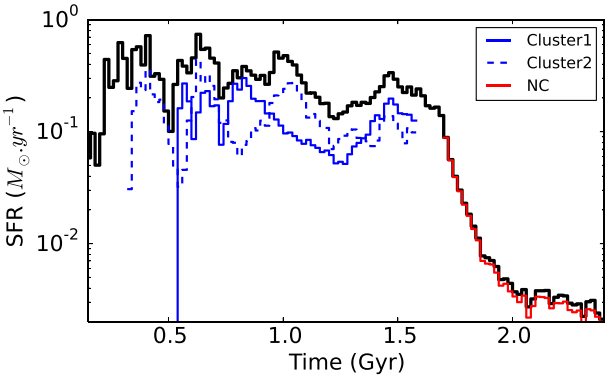

Figure 8. Contribution of Cluster1 (solid), Cluster2 (dashed) and their merger (NC, red) in the total SFR (black). The latter is dominated by Cluster1 and Cluster2 and by the NC in the end. Cluster1 and Cluster2 cannot be distinguished from each other after $t = 1.6$ Gyr.

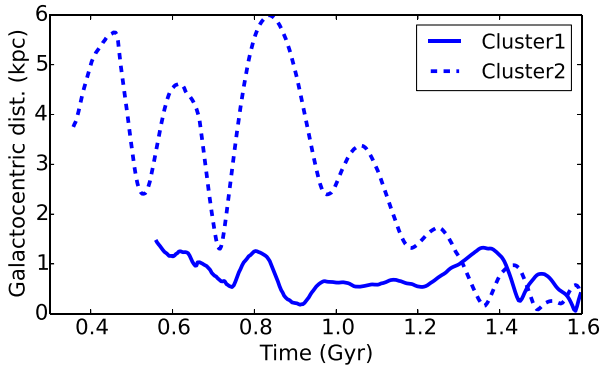

Figure 9. Galactocentric distance of Cluster1 (solid) and Cluster2 (dashed). The galactic centre is defined as the centre of mass of particles (stars + DM).

probability distribution function (PDF) within the central kpc, during the merger phase. Before the merger, the PDF yields a classical lognormal shape corresponding to supersonic ISM (Vazquez-Semadeni 1994), and a power-law tail for $\rho \gtrsim 2000$ cm^{-3} indicating self-gravitating gas (Elmegreen 2011; Renaud et al. 2013). The collision between the gas clouds around the NC and Cluster2 generates an excess of dense gas ($>10^4$ cm^{-3}), leading to a starburst localized in the central 25 pc. In the meantime, the tidal interaction strips gas from the outskirts of the clouds, thus depleting gas at intermediate density (∼100 cm^{-3}). The dependence of star formation on $\rho^{3/2}$ implies that the depletion at intermediate densities approximately balances the central excess at high densities. Thus, despite the central mini starburst, the net SFR remains almost constant over 100 pc. After the merger, the central star formation has consumed a large fraction of the dense gas, and the associated feedback disperses most of the gas left in this volume. This lack of dense gas reduces significantly the SFR to a few 10^{-3} M$_\odot$ yr^{-1}, thus almost quenching star formation in the NC.

3.3 Merger: a mandatory process?

To test the importance of the merging step in the formation scenario of the NC, we artificially remove the stars associated with Cluster2 from the simulation, before it interacts with cluster1 ($t = 500$ Myr, i.e. when Cluster2 has formed about half of its final mass). This procedure is sufficient to prevent the further formation of a massive

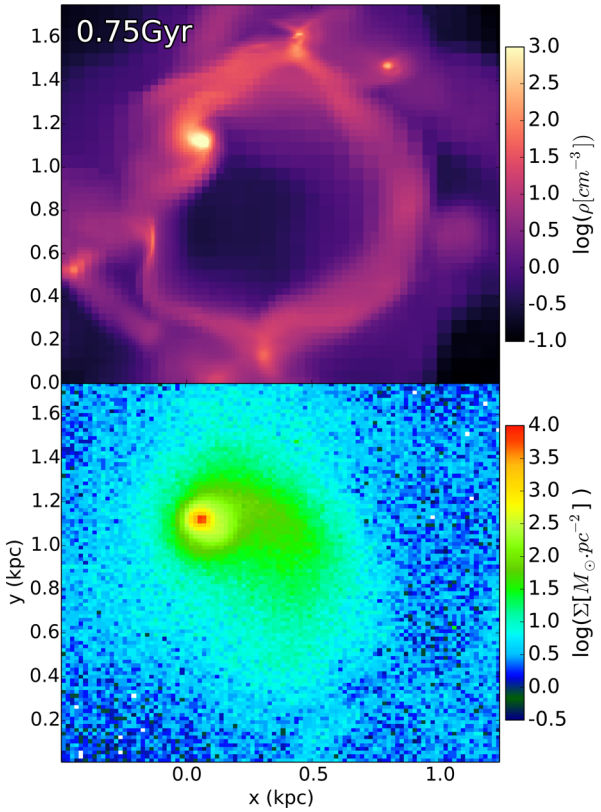

Figure 10. Maps of the gas (top) and new stars (bottom) densities. The shell from the SN which explodes 5 Myr before is visible on the gas density map. The asymmetric extension of Cluster1 (on the right) is the combined result of its orbit and of the SN blast.

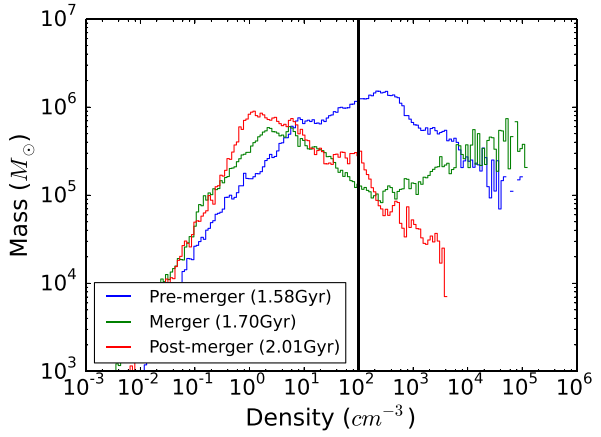

Figure 11. PDFs inside a 1 kpc × 1 kpc × 1 kpc centred on the NC or centre of mass of the system (Cluster1–Cluster2) before they merge. The vertical line represents the density threshold for the SF.

cluster, and does not alter the large-scale dynamics of the rest of the galaxy.

In this alternative simulation, a cluster similar to Cluster1 still forms at $t = 800$ Myr and reaches the centre in about the same amount of time, namely 300 Myr. The NC forms as described in Section 3.1. We then let the NC evolve for 700 Myr ($t = 1.7$ Gyr). However, the absence of another massive cluster being able to merge with the NC voids the second step of our scenario. All the effects associated with the merger phase (recall Section 3.2) are thus missing in the further growth of the NC. Namely,

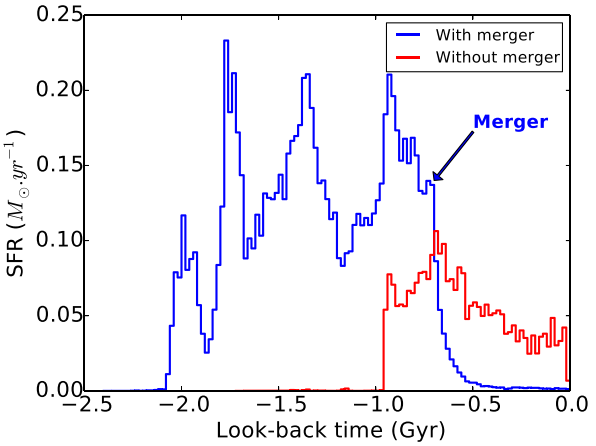

Figure 12. Star formation history 700 Myr after the formation of the final NC ($t = 0$). Only the stars within a radius of 100 pc centred on the NC are considered. When the NC experiences a merger (arrow at $t = -0.7$ Gyr), the stellar population of the NC is a mix of that of Cluster1 (formed at $t = -1.9$ Gyr) and that of Cluster2 (formed at $t = -2.1$ Gyr). Star formation is quenched after the event. When there is no merger, the stellar populations is only that of the NC progenitor (formed at $t = -0.9$ Gyr).

(i) The depletion of the dense gas reservoir does not occur and the NC continuously forms stars. This affects the star formation history of the NC as shown in Fig. 12. In the merger scenario, both NC cluster progenitors form stars during their entire lifetimes, until star formation gets quenched at the time of the collision. This leads to the mixing of stellar populations with different ages, and the lack of a young population.

(ii) The angular momentum redistribution noted during the merger does not happen and the NC maintains an almost spherical morphology (axis ratio of 0.8), as opposed to the flattened shape visible in Fig. 5.

(iii) Without merger, there is no increase of the angular momentum and the resulting NC exhibits a lower amplitude rotation than in the case of a merged system: the difference in angular momentum is approximately of a factor of 10.

(iv) The resulting NC is less massive but has a similar size (5×10^7 M$_\odot$ and 40 pc in our cases) without the merger step.

Note that the first three points could be used as observational diagnostics to establish the formation scenario of real NCs.

This demonstrates that the merger step is not mandatory for the formation of the NC, but can significantly alter the properties of the NC when it takes place.

4 CLUSTER POPULATIONS

4.1 Cluster disruption

In our fiducial simulation, Cluster1 and cluster2 represent 15 per cent of the new stars of the disc, and set the dynamics of their surroundings. The rest of the star cluster population thus experiences several interactions with Cluster1, Cluster2 and the NC, and some get disrupted by tidal forces. Signatures of tidal disruptions are visible throughout the simulation (see e.g. bottom-left panel of Fig. 5).

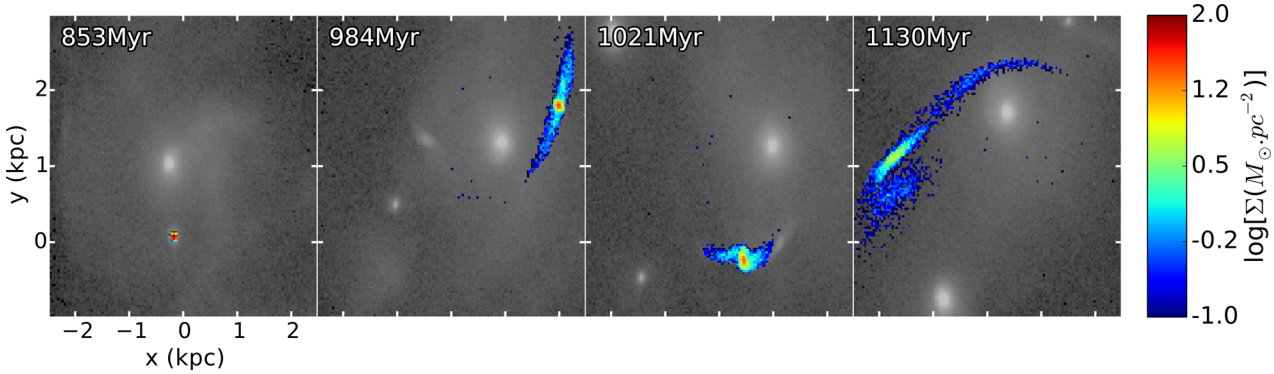

Figure 13. Disruption of a cluster through time. The galactic stellar background is shown in grey scale (Cluster1 is the closest to centre of the maps). The colour scale represents the surface density of the stars initially detected in the cluster (first panel). Interactions between clusters in the galaxy (mainly Cluster1 and Cluster2) generate tidal tails and eventually lead to the dissolution of the low-density cluster.

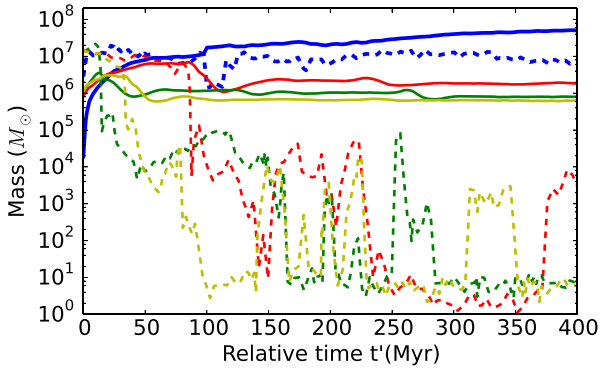

Figure 14. Evolution of the stellar (solid) and gas (dashed) mass of the clusters surviving the presence of the NC, compared to that of Cluster1 (blue). We measure the gas mass in a cube of 50 pc centred on the cluster. Each colour corresponds to one cluster (A in red, B in green and C in yellow). As in Fig. 7, the time is relative, with $t' = 0$ marking the earliest detection of each cluster.

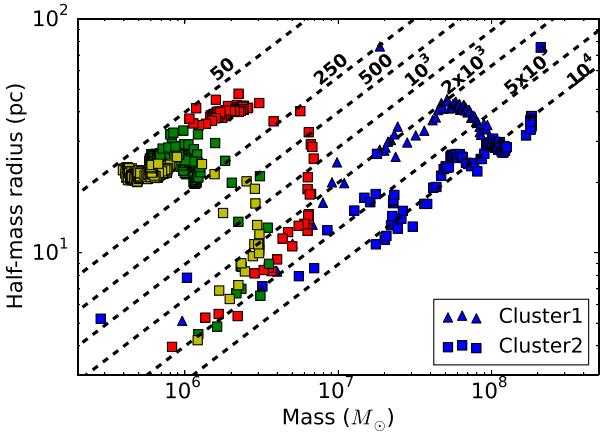

Figure 15. Evolution of size and mass of all clusters detected at the end of the simulation. Colours are as in Fig. 14. The dashed lines follow constant surface density values in $M_\odot\,pc^{-2}$.

One example of this disruption process is shown in Fig. 13, where we monitor the stars of one cluster during about 300 Myr, until its complete destruction by tidal forces. At $t = 853$ Myr (first panel of Fig. 13), a bound cluster is detected 1 kpc away from Cluster1. The tidal interaction between Cluster1 and this $\sim 10^5\,M_\odot$ cluster induces tidal tails (second panel of Fig. 13). Subsequent interactions, including one with the approaching Cluster2, accelerate the disruption, finally leading to complete dissolution. The tidal features can still be detected as elongated overdensities for another 250 Myr after the dissolution, until the surface density contrast with the background becomes too low. This situation is similar for other less dense clusters. This shows the key role of massive clusters such as Cluster1 and Cluster2 in the evolution of the cluster population as a whole, accelerating the disruption of the most fragile objects.

4.2 Surviving clusters

As illustrated in Fig. 5, some clusters survive the disruptive presence of the NC. We detect three of these clusters (named A, B and C) keeping a constant mass for most of the simulation ($\sim 10^6\,M_\odot$, see Figs 14 and 15). However, their mass evolutions strongly differ from that of Cluster1 and Cluster2. Their growth phase only lasts about 10–40 Myr. This star formation activity leads to a rapid injection of SN energy into the ISM, but their lower density is not enough to retain the feedback winds, which thus depleting the gas reservoir mass by one to three orders of magnitude (in mass). Fig. 16 illustrates this by showing the evolution of the gas density PDFs in the regions of the clusters.

For clusters A, B and C, stellar feedback happens to truncate the PDFs close to the density threshold associated with star formation, thus preventing further star formation. The rapid gas removal by stellar feedback in clusters A, B and C has a significant impact on the local gravitational potential. The least bound stars are then ejected from the clusters (Hills 1980; Boily & Kroupa 2003). This lowers the clusters masses by a factor of 2–7 and their surface densities by one order of magnitude (see Fig. 15), which then remain roughly constant until the end of the simulation. The mass of the gas reservoirs shows fluctuations over time. A sharp increase of the gas mass can lead to an increase of the clusters mass for a short period. This is for example the case for cluster B at $t' = 250$ Myr in Fig. 14. The stellar mass of the cluster then decreases as the least bound stars are ejected from the cluster.

The main difference between NC progenitors and the rest of the cluster population is then their ability to retain a significant fraction of their stellar mass. In Cluster1 and Cluster2, the injected feedback energy is not high enough to significantly alter the existing gas reservoir. By keeping a dense gas reservoir, they can further form stars and become even more massive and resistant to subsequent

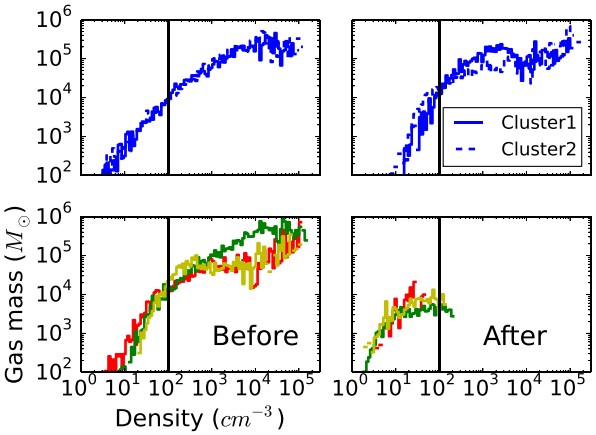

Figure 16. Gas density PDFs in regions of 50 pc centred on the clusters 5 Myr before (left-hand column) and after (right-hand column) the removal of gas by SN-blasts. The blue curve shows the evolution for Cluster1 and Cluster2 for reference. The vertical lines show the density threshold above which gas can be converted into stars.

tidal disruptions induced along their orbits. Altogether, these points indicate that the low-density clusters have a much lower probability to survive and become seeds for an NC, in contrast with e.g. Cluster1 (see Section 3.1).

The dynamical friction time of clusters A, B and C is much longer, of the order of tenths of Gyr, since the dynamical friction time is inversely proportional to the cluster mass. Therefore they cannot contribute to the building of the NC through mergers within several Gyr, unlike Cluster2 (see Section 3.2).

5 DISCUSSION AND CONCLUSION

Using hydrodynamical simulations of an isolated gas-rich dwarf galaxy, we propose a 'wet migration' scenario for the formation of NCs. The main steps are as follows (see also Fig. 1).

(i) A population of star clusters forms across the galactic disc.
(ii) Clusters dense enough to retain a gas reservoir around them maintain a star formation activity for a few 100 Myr, which steadily increases their masses.
(iii) These clusters lose orbital energy through dynamical friction and interactions with the rest of the disc and migrates to the centre to form an NC.
(iv) The NC eventually experiences (wet) mergers with other dense clusters, increasing its mass and quenching its star formation activity.

The last step is not mandatory for the formation of the NC but strongly affect its properties (mass, shape, star formation history), as discussed in Section 3.3.

The other star clusters in the galaxy have lower initial densities, which affects their early evolution and tells them apart from the NC progenitors. They are either tidally disrupted by the central structures (including the NC itself) or have high orbital angular momentum which prevents them to interact with the NC and participate to its build-up.

By comparing the properties of the NC modelled with that of the observed population, Fig. 17 shows that our simulation is in line with the observed scaling relations (e.g. Georgiev et al. 2016). Our NC lies in the high mass and size regime (40 pc and 5×10^7 $M_\odot$ without

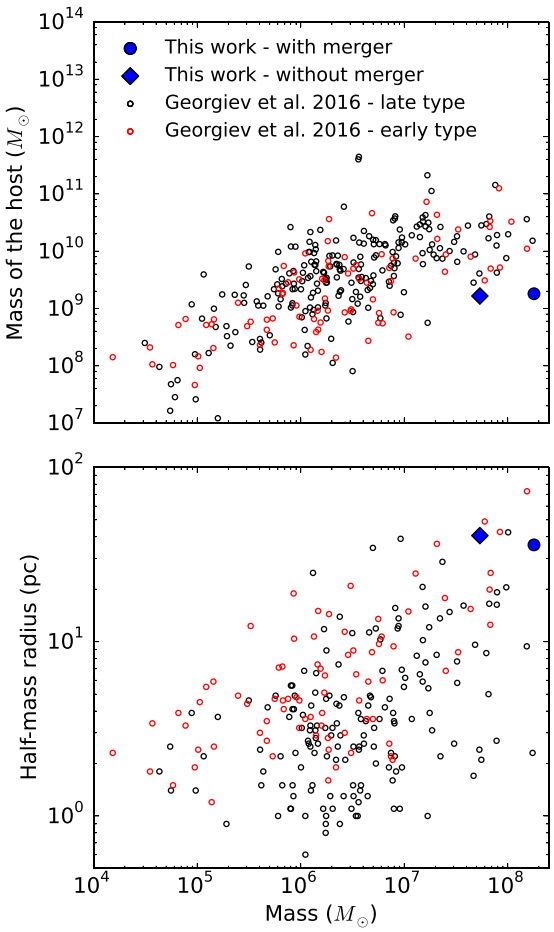

Figure 17. Position of the NCs formed in our simulation on the galaxy mass–observed cluster mass scaling relation (top) and in a size–mass diagram (bottom).

merger, and 35 pc and 1.8×10^8 $M_\odot$ with merger). Although well within the dispersion of observational data, NCs in this mass range would be preferentially detected in slightly more massive galaxies. However, galaxies with different masses are likely to play different roles on the formation process of their NCs, as underlined by previous works. Observations by den Brok et al. (2014) favour the migration scenario in the low-mass regime ($\lesssim 10^{9-10}$ $M_\odot$, see also the theoretical confirmation by Arca-Sedda & Capuzzo-Dolcetta 2014). The relative important of *in situ* star formation increases with galactic mass, as showed by Antonini et al. (2015), suggesting that massive galaxies are more prone to drive gas flows towards the NC and fuel *in situ* star formation than their low-mass counterparts.

Such gas flows are related to kpc-scale dynamics of the galactic disc, in particular the presence of substructures. For instance, torques from bars are well known to drive gas infall towards the galactic centre (Roberts, Huntley & van Albada 1979; Athanassoula 1992; García-Burillo et al. 2014; Emsellem et al. 2015). This process would then supply the NC with gas and maintain its star formation activity over long time-scales. Ongoing star formation would then occur preferentially in the plane of the galactic disc (Seth et al. 2006; Böker 2010; Feldmeier-Krause et al. 2015), thus leading to a flattened NC. A similar morphology is predicted by our model in the case of a cluster merger. However in our case, the merger quenches star formation. Therefore, the absence of young

stars in a flattened NC favours our merger scenario, while a young population denotes *in situ* formation.

We also note that spiral arms would lead to star cluster formation providing more candidates for dry or wet mergers with the NC. It is however not clear whether these potential NC progenitors would survive the radial migration through spirals and bars (Fujii & Baba 2012). Probing these processes would require to model galaxies of different masses and disc stabilities over several rotation periods to allow for the formation and evolution of substructures.

Accounting for the cosmological context would also be key for replenishing the gas reservoir with low-metallicity gas (through cold gas accretion), and/or triggering the formation and destruction of spirals and bars (see e.g. Kraljic, Bournaud & Martig 2012). Over such long time-scales, and particularly in the redshift range considered here ($z \sim 2$–3), it is likely that a dwarf galaxy like that modelled here would experience interactions with its environment, either with other galactic systems or with the intergalactic medium. Depending on the state of the cluster (growing seed or fully formed NC), we expect the outcome of these interactions to vary. On one hand, the perturbations will likely disturb the orbit of the seed. On the other hand, the dwarf may suffer from tidal stripping and its NC, if already formed, may become an ultracompact dwarf galaxy (see e.g. Pfeffer & Baumgardt (2013) or Norris et al. (2015). The nature of the perturbation is also to be considered. A dwarf within a cluster-like environment will likely experience processes such as gas stripping or ram pressure. The resulting impact on the gas content can thus be significant, with either boosting or slowing down the growth of the NC progenitors. Along the same lines, mergers would possibly induce dramatic changes both in the morphology and star formation history of the galaxies. The migration and growth of an NC seed should be examined further in such contexts.

Such time-lapses become comparable to the relaxation time-scales of typical NCs ($\sim 10^9$ yr, although the massive ends of the population, including our case yield much longer time-scales $\sim 10^{11}$ yr; see also Seth et al. 2006). Following the co-evolution of the NC and its host over such long periods would then require to consider collisional processes to properly treat the internal physics. Among other internal mechanisms, a full treatment of stellar evolution would provide insights on the formation of stellar mass black holes in the NC and its progenitor clusters. Then, the possible merger step in our scenario would represent an important channel in the formation of intermediate and possibly supermassive black holes in galactic centres (Seth et al. 2006; Antonini et al. 2015), potentially followed by an active phase of the galactic nucleus.

ACKNOWLEDGEMENTS

We wish to thank the anonymous referee for the helpful comments and suggestions that improved the paper. This research was supported by the DFG cluster of excellence 'Origin and Structure of the Universe' (www.universe-cluster.de). We acknowledge the support by the DFG Cluster of Excellence 'Origin and Structure of the Universe'. The simulations have been carried out on the computing facilities of the Computational Centre for Particle and Astrophysics (C2PAP). FR acknowledges support from the European Research Council through grant ERC-StG-335936.

REFERENCES

Andersen D. R., Walcher C. J., Böker T., Ho L. C., van der Marel R. P., Rix H.-W., Shields J. C., 2008, ApJ, 688, 990
Antonini F., 2013, ApJ, 763, 62
Antonini F., Barausse E., Silk J., 2015, ApJ, 812, 72
Arca-Sedda M., Capuzzo-Dolcetta R., 2014, MNRAS, 444, 3738
Athanassoula E., 1992, MNRAS, 259, 345
Behroozi P. S., Wechsler R. H., Conroy C., 2013, ApJ, 770, 57
Boily C. M., Kroupa P., 2003, MNRAS, 338, 665
Böker T., 2010, in de Grijs R., Lépine J. R. D., eds, Proc. IAU Symp. 266, Star Clusters: Basic Galactic Building Blocks Throughout Time and Space. Cambridge Univ. Press, Cambridge, p. 58
Böker T., Laine S., van der Marel R. P., Sarzi M., Rix H.-W., Ho L. C., Shields J. C., 2002, AJ, 123, 1389
Carollo C. M., Stiavelli M., Mack J., 1998, AJ, 116, 68
Carson D. J., Barth A. J., Seth A. C., den Brok M., Cappellari M., Greene J. E., Ho L. C., Neumayer N., 2015, AJ, 149, 170
Chandrasekhar S., 1943, ApJ, 97, 255
Cole D. R., Debattista V. P., Varri A. L., Hartmann M., Seth A. C., 2016, preprint (arXiv:1605.02881)
Côté P. et al., 2006, ApJS, 165, 57
Courty S., Alimi J. M., 2004, A&A, 416, 875
Daddi E. et al., 2010, ApJ, 713, 686
den Brok M. et al., 2014, MNRAS, 445, 2385
Dubois Y., Teyssier R., 2008, A&A, 477, 79
Eisenstein D. J., Hut P., 1998, ApJ, 498, 137
Elmegreen B. G., 2011, ApJ, 731, 61
Emsellem E., Monnet G., Bacon R., 1994, A&A, 285, 723
Emsellem E., Renaud F., Bournaud F., Elmegreen B., Combes F., Gabor J. M., 2015, MNRAS, 446, 2468
Feldmeier-Krause A. et al., 2015, A&A, 584, A2
Ferrarese L. et al., 2006, ApJ, 644, L21
Ferrero I., Abadi M. G., Navarro J. F., Sales L. V., Gurovich S., 2012, MNRAS, 425, 2817
Fujii M. S., Baba J., 2012, MNRAS, 427, L16
García-Burillo S. et al., 2014, A&A, 567, A125
Georgiev I. Y., Böker T., 2014, MNRAS, 441, 3570
Georgiev I. Y., Böker T., Leigh N., Lützgendorf N., Neumayer N., 2016, MNRAS, 457, 2122
Graham A. W., 2012, MNRAS, 422, 1586
Hartmann M., Debattista V. P., Seth A., Cappellari M., Quinn T. R., 2011, MNRAS, 418, 2697
Hills J. G., 1980, ApJ, 235, 986
Kraljic K., Bournaud F., Martig M., 2012, ApJ, 757, 60
Milosavljević M., 2004, ApJ, 605, L13
Mo H., van den Bosch F. C., White S., 2010, Galaxy Formation and Evolution. Cambridge Univ. Press, Cambridge
Monnet G., Bacon R., Emsellem E., 1992, A&A, 253, 366
Navarro J. F., Frenk C. S., White S. D. M., 1996, ApJ, 462, 563
Neumayer N., Walcher C. J., 2012, Adv. Astron., 2012, 15
Norris M. A., Escudero C. G., Faifer F. R., Kannappan S. J., Forte J. C., van den Bosch R. C. E., 2015, MNRAS, 451, 3615
Pfeffer J., Baumgardt H., 2013, MNRAS, 433, 1997
Pfeffer J., Griffen B. F., Baumgardt H., Hilker M., 2014, MNRAS, 444, 3670
Renaud F. et al., 2013, MNRAS, 436, 1836
Renaud F., Bournaud F., Duc P.-A., 2015, MNRAS, 446, 2038
Roberts W. W., Jr, Huntley J. M., van Albada G. D., 1979, ApJ, 233, 67
Rossa J., van der Marel R. P., Böker T., Gerssen J., Ho L. C., Rix H.-W., Shields J. C., Walcher C.-J., 2006, AJ, 132, 1074
Scott N., Graham A. W., 2013, ApJ, 763, 76
Seth A. C., Dalcanton J. J., Hodge P. W., Debattista V. P., 2006, AJ, 132, 2539
Seth A., Agüeros M., Lee D., Basu-Zych A., 2008, ApJ, 678, 116
Teyssier R., 2002, A&A, 385, 337
Spitzer Jr, L.Tremaine S. D., Ostriker J. P., 1975, ApJ, 196, 407
Turner M. L., Côté P., Ferrarese L., Jordán A., Blakeslee J. P., Mei S., Peng E. W., West M. J., 2012, ApJS, 203, 5
Vazquez-Semadeni E., 1994, ApJ, 423, 681

This paper has been typeset from a TEX/LATEX file prepared by the author.